X-RAY SPECTROMETRY

https://doi.org/10.1070/QEL17074

Flat-field VLS spectrometer for a wavelength range 50 – 275 Å

A.O. Kolesnikov, E.A. Vishnyakov, A.N. Shatokhin, E.N. Ragozin

Abstract. **A flat-field VLS spectrograph for a wavelength range ~50–275 Å with an average linear dispersion of 0.18 mm Å^{-1}, which makes use of a grazing-incidence varied line-space (VLS) grating, was calculated and implemented (a spectrograph of Harada class). To fabricate the VLS grating by interference lithography technique, an algorithm was developed for calculating the writing configuration with an auxiliary aberrating mirror (the solution of the inverse problem of interference lithography). The spectrograph was put to a test and line spectra were recorded from the laser-produced plasma of lithium fluoride and teflon targets, which were excited by a focused laser beam (0.5 J, 8 ns, 1.06 μm). A resolving power $\lambda/\delta\lambda = 800$ was demonstrated in a wavelength region of 135 Å.**

Keywords: *soft X-rays, flat-field spectrograph, laser plasma, spherical VLS grating, interference lithography.*

1. Introduction

Beginning with the 1980s, the world has seen the development of flat-field soft X-ray (SXR) diffraction spectrometers with near-normal incidence of diffracted beams on a detector. This makes spectrometers of this class compatible with modern CCD detectors. The first instrument of this class was implemented by T. Harada [1, 2], in which the flat field spanned a region from 50 to 200 Å. He made use of a mechanically ruled spherical (R = 5649 mm) varied line-space (VLS) grating with a ruled area of 50 × 30 mm and a central groove density p_0 = 1200 mm^{-1}, the grating spacing varying from 0.69 to 0.99 μm across the aperture. More recently, flat-field spectrometers were developed for other spectral ranges, including spectrometers with a higher resolving power. For instance, in the Lawrence Livermore National Laboratory (LLNL), USA, use is made of flat-field spectrograph for a range of 10–50 Å [3, 4].

Spherical VLS gratings have also underlain the realisation of imaging slitless spectrographs intended for recording high-order laser harmonics and their angular distribution. In this case, use was made of the Harada grating with p_0 = 1200 mm^{-1} [5] as well as of the grating developed by M. Koike et al. (R = 15920 mm, p_0 = 2400 mm^{-1}) [6]. VLS gratings are also employed in SXR emission spectroscopy (SXES) combined with an electron microscope [7] (see also review [8]). The key component of a flat-field spectrometer is a VLS grating. Nowadays work is actively underway to make VLS gratings and VLS spectrometers based on them, with emphasis being placed on extending the spectral operating range towards tender X-rays ($\hbar\omega \approx$ 1.5–6 keV) [9] and increasing the spectral resolving power [10]. Another promising area is the development of high-resolution imaging VLS spectrometers comprising a concave normal-incidence multilayer mirror and a plane VLS grating [11–13].

Here we set ourselves the task to make a compact flat-field VLS spectrometer for a range $\lambda \approx$ 50–275 Å. For a technique of VLS grating fabrication, we selected interference lithography. This technique is underlain by the calculation of the writing configuration that realises the desired interference fringe density dependence across the exposed substrate aperture (the future grating). Each new VLS spectrometer, which is designed for a specific problem and a specific radiation source, calls for a unique grating with its unique law of grating spacing variation across the aperture. And therefore the second task, and an even more important one, was to gain the capacity to calculate the writing configurations for a broad class of VLS gratings. This problem was solved by the example of a half-metre flat-field VLS spectrometer.

2. Spectrograph configuration

Three Harada-type spectrographs of length approximately 0.25, 0.5 and 1.5 m were designed in our earlier work [14] for operation in the ranges 90–250, 50–275 and 20–110 Å, respectively. Selected for implementation in the present work was the half-metre device with a plate scale of 6.28 Å mm^{-1} at a wavelength of 150 Å. Near λ = 150 Å the theoretical resolving power corresponding to two detector pixels amounts to about 920. Figure 1 is a schematic representation of the instrument. The groove density of the VLS grating is described by the polynomial

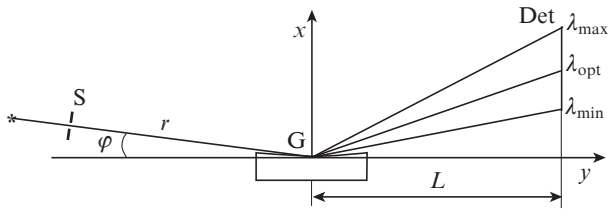

Figure 1. Schematic of the spectrograph: (G) VLS grating centre, (S) entrance slit, (Det) detector.

A.O. Kolesnikov, A.N. Shatokhin Lebedev Physical Institute, Russian Academy of Sciences, Leninsky prosp. 53, 119991 Moscow, Russia; Moscow Institute of Physics and Technology (National Research University), Institutskii per. 9, 141701 Dolgoprudnyi, Moscow region, Russia; e-mail: alexey6180@gmail.com;
E.A. Vishnyakov, E.N. Ragozin Lebedev Physical Institute, Russian Academy of Sciences, Leninsky prosp. 53, 119991 Moscow, Russia

Received 10 June 2019; revision received 25 July 2019
Kvantovaya Elektronika **49** (11) 1054–1058 (2019)
Translated by E.N. Ragozin

$$p(y) = p_0 + p_1 y + p_2 y^2 + p_3 y^3, \quad (1)$$

where p_0 is the groove density at the centre of the grating aperture. The groove density (1) should vary from 1027.5 to 1427.5 grooves mm^{-1} between the edges of the 50-mm wide aperture. The main design parameters of the spectrograph and the VLS grating are collected bellow.

Radius of curvature R of spherical grating/mm	6000
Grating diameter D/mm	60
p_0/mm^{-1}	1200
p_1/mm^{-2}	8.0
p_2/mm^{-3}	0.044
p_3/mm^{-4}	2.28×10^{-4}
Grazing incidence angle φ/deg	3.0
Wavelength λ_{opt} of aberration compensation/Å.	125
Entrance slit – grating centre distance/mm	252
L/mm	250

After formulating the requirements on the instrument parameters (the spectral range, resolution and length) and selecting the main configuration parameters (φ, p_0, etc.) it is necessary to perform an analytical calculation of the paraxial spectral focus and select p_1, whereby the working portion of the spectral focal curve between λ_{min} and λ_{max} is best approximated by a line segment. Next, it is required to find the optimal detector (Det) position that minimises the departure of its sensitive surface from the analytically found plane portion of the focal surface. After that, numerical ray tracing is used to construct the spectral images of the point monochromatic sources positioned in place of the entrance slit (see Ref. [14]). In doing this we define more precisely the main configuration parameters and find coefficients p_2 and p_3 such that minimise the aberration of meridional coma and spherical aberration in the given portion of the spectrum. This algorithm (the upper cycle in Fig. 2) is a converging self-consistent procedure, which serves to uniquely define the requirements on the VLS grating.

In the selection of the method of VLS grating fabrication, we decided in favour of interference lithography. The stages of grating fabrication are described in Section 3. It is pertinent to note that a correction of the optical configuration of the instrument may be required in case the resultant parameters p_i do not coincide with the design ones. Section 4 describes the assembly, alignment, and testing of the instrument by recording the line spectra of multiply charged ions. The complete sequence of the operations in the development of the instrument is diagrammed in Fig. 2.

3. VLS grating fabrication

The fabrication of a VLS grating by interference lithography is preceded by the design of the optical 'writing' configuration (by solution of the inverse problem of interference lithography). The writing configuration is calculated with the inclusion of the wavelength of the writing laser and the dimensions of the lithographic table. The writing configuration must produce an interference pattern where the spatial frequency of interference fringes on the substrate aperture is described by polynomial (1) with the previously found coefficients p_1, p_2 and p_3. Also of significance is the radius of curvature of the interference fringes.

For VLS grating fabrication we selected a writing scheme consisting of two coherent sources and one auxiliary oblique-incidence spherical mirror, which introduces controllable aberrations in the wave front of one of the interfering beams (Fig. 3).

To design the writing scheme of this type, a three-stage algorithm was developed. The first stage involved the inversion of the direct problem of interference lithography, which was comprehensively set forth in Ref. [15]. The inverted solution yielded the approximate positions of the point sources and the mirror, which were then used as the initial approximation in the finding of the exact solution at the optimisation stage. This optimisation is possible due to the existence of degrees of freedom in the writing configuration, i.e. the existence of a continuous set of parameter values of the writing configuration corresponding to the same polynomial (1). The optimisation involves minimisation of the functional of the following form:

$$\int_{y_{min}}^{y_{max}} [p(y) - p^*(y)]^2 \exp\left(-\frac{y^2}{2y_{opt}^2}\right) dy + a_1 \exp\left(-\frac{r_{groove}}{r_{opt}}\right)$$

$$+ a_2(\exp(\Delta y - \Delta y^*) - 1) + a_3(\exp(\Delta z - \Delta z^*) - 1), \quad (2)$$

where $p(y)$ is the groove density; $\Delta y = y_{max} - y_{min}$ is the grating width; Δz is the grating height; r_{groove} is the radius of curvature of the grooves; and $a_i (i = 1-3)$, y_{opt} and r_{opt} are parameters, which control the optimisation procedure. Asterisks denote the target values of the quantities, while asterisk-free quantities denote those resulting from the writing configuration, which were obtained by simulating the writing configuration in the ray approximation. The first term of the functional is responsible for the precision of adherence to the requisite groove density $p(y)$, the second one for lowering the curvature of interference fringes, while the third and the fourth for the proximity to the desired grating aperture. The result of optimisation procedure is exemplified in Fig. 4.

The completion of optimisation is followed by verification of the writing configuration. Simulated for this purpose is the operation of the spectrograph equipped with the grating corresponding to the writing configuration: numerical ray tracing is used to construct the spectral images of a point monochromatic source positioned in place of the entrance slit of the instrument. At this stage, it is possible to reconsider the grating writing configuration as well as the spectrograph configuration.

Spherical substrates of diameter 60 mm (R = 6000 mm) and an auxiliary aberrating mirror of diameter 150 mm (R = 500 mm) were made of fused silica KU-1 (SOTVEKS Ltd, Moscow). Spherical VLS gratings were made at the Scientific and Production Association 'State Institute of Applied Optics' (Kazan) by 0.53 μm interference lithography procedure and coated with a reflective gold layer. Then, at the Lebedev Physical Institute the real dependence $p_{exp}(y)$ was measured from the diffraction of 0.63 μm laser radiation. The measured dependence turned out to be practically indistinguishable from the desired one $p(y)$ (see Table 1 for the design parameters of grating) (Fig. 5).

4. Spectrograph implementation and recording of line spectra of multiply charged ions from laser-produced plasma

The spectrograph elements were mounted on a rigid duraluminium plate 0.6 m in length (Fig. 6). For a detector, we used

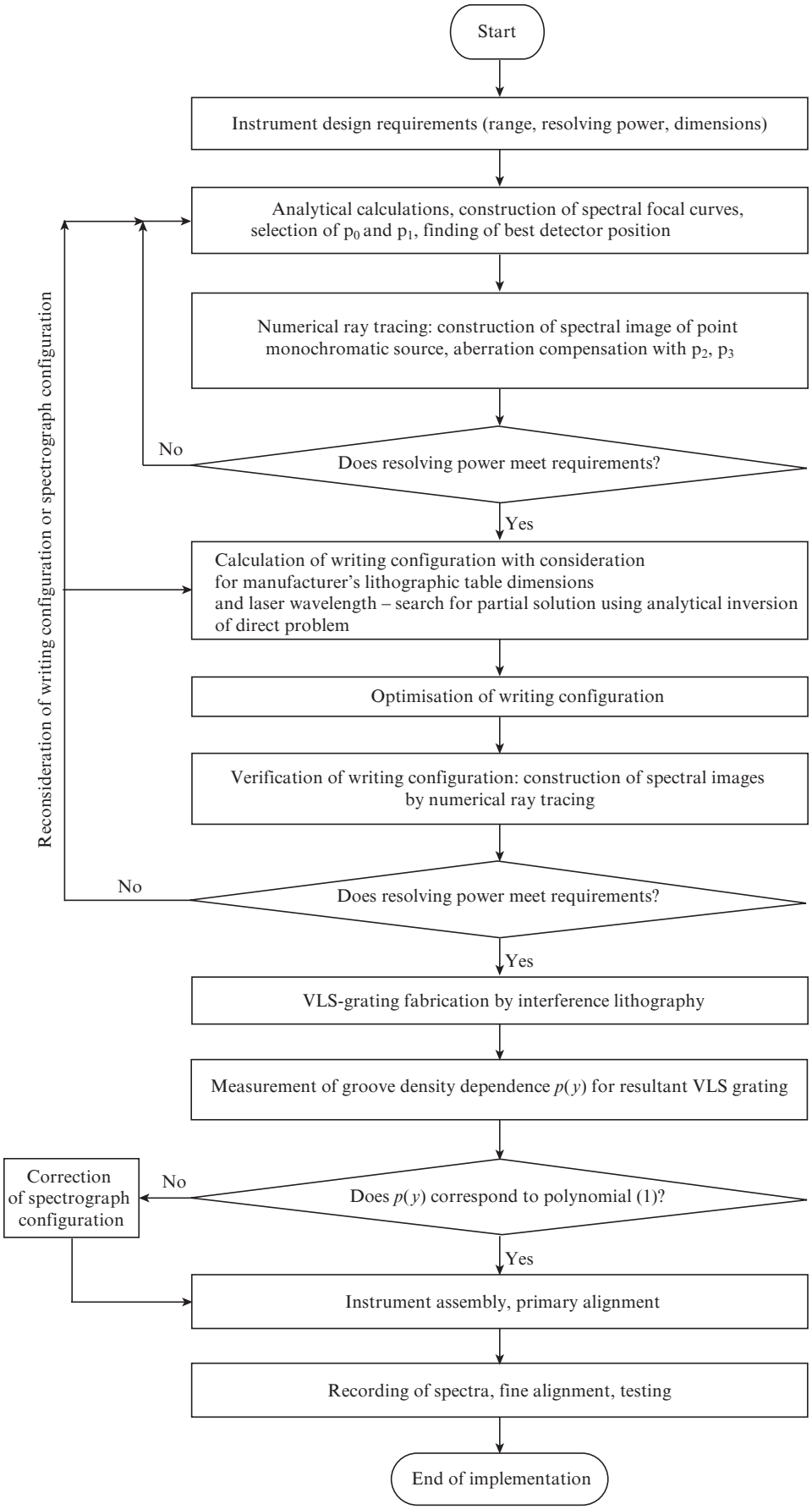

Figure 2. Block diagram describing the VLS-spectrometer development cycle.

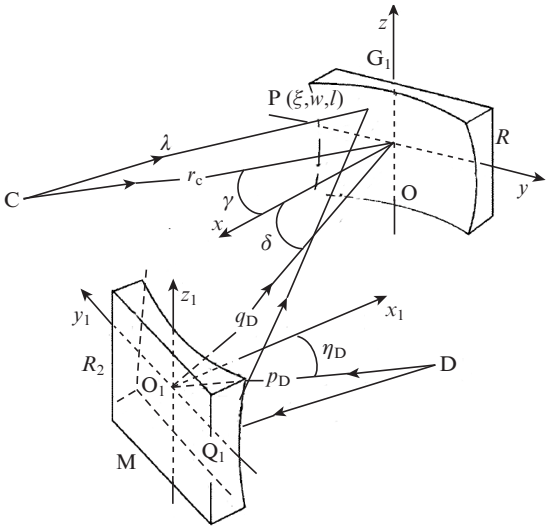

Figure 3. Interference lithography configuration with an auxiliary spherical mirror [15]: (C) and (D) point coherent monochromatic sources; (G_1) diffraction grating blank; (M) auxiliary spherical aberrating mirror of radius R_2; $\gamma < 0$, $\delta > 0$, and $\eta_D < 0$ are the central-ray angles of incidence on the grating blank and the aberrating mirror; r_C, p_D and q_D are the distances between the source C and the blank centre, the source D and the mirror, the blank centre and the mirror, respectively.

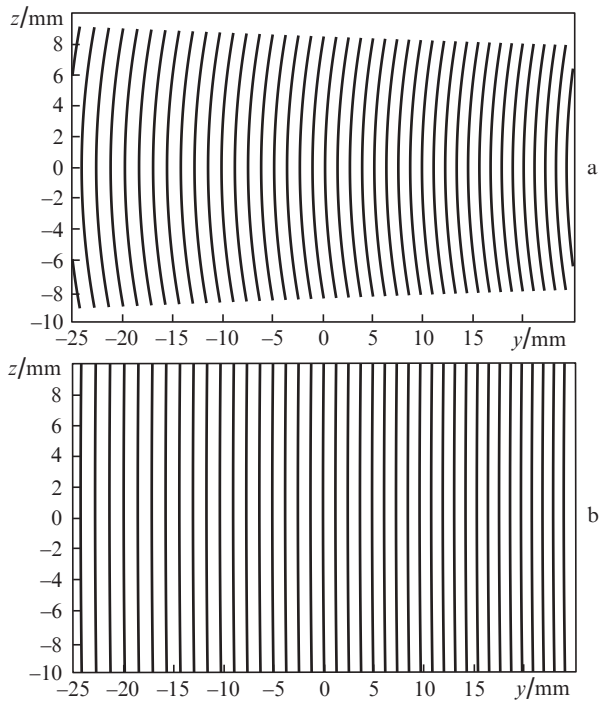

Figure 4. Example of optimisation of the VLS-grating writing configuration, which lengthened the radius of groove curvature from 32 (a) to 500 mm (b) and increased the aperture with retention of the desired dependence $p(y)$.

a backside-illuminated CCD array (2048 × 1024) with square pixels of size 13 μm and a sensitive area length of 27 mm, whose responsivity was measured in Refs [16,17]. The grating was mounted on a high-precision motorised rotary stage and the detector was placed on a one-dimensional motorised translation stage, which were computer-controlled. The primary alignment of the spectrograph was performed using a He–Ne laser

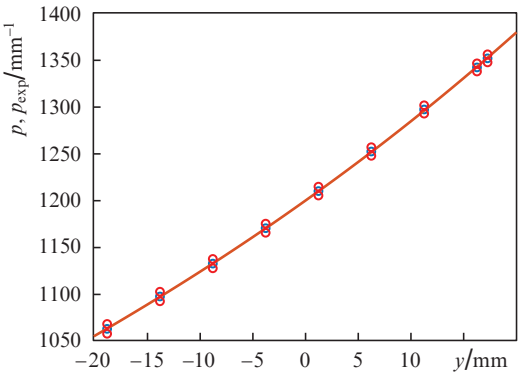

Figure 5. Design, $p(y)$, (curve) and measured, $p_{exp}(y)$, groove density of the VLS grating.

(0.63 μm). For a test, the spectrometer was placed in a cylindrical vacuum chamber 0.9 m in diameter and 3.8 m in length, which was equipped with an oil-free pump system and pumped to a residual pressure of $\sim 10^{-5}$ Torr. Owing to the high-precision motorised positioners from Vicon-Standa Ltd. (Lithuania), the fine final alignment was carried out by recording the line spectra of multiply charged ions, when the chamber was evacuated.

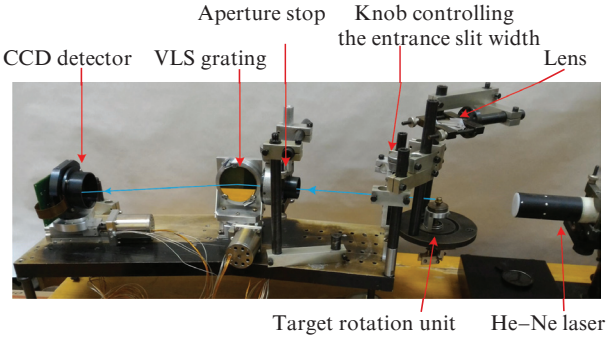

Figure 6. Flat-field VLS spectrometer for a range of 50–275 Å assembled on a rigid 0.6-m long plate.

The spectra of laser-produced plasma were excited by laser pulses (0.5 J, 8 ns, 1.06 μm) focused with an $f = 110$ mm lens on a solid target. The target surface lay in the dispersion plane of the instrument.

Figure 7 displays the photograph of the spectrum obtained in one laser shot in the irradiation of a LiF target, which contains the lines of Li III and F V–F VII ions. The halfwidths (FWHM) of isolated lines are equal to two detector pixels. The practical spectral resolution is limited by the spatial detector resolution and is numerically equal to the product of the plate scale and the doubled pixel size of the CCD array (26 μm). Since the plate scale is wavelength-dependent, the spectral resolution also depends on the wavelength (Fig. 8). The theoretical resolving power corresponding to two detector pixels is wavelength-dependent and varies from 550 in the 60 Å region to 1170 in the 220 Å region.

In the vicinity of $\lambda = 135$ Å there are close F VII ion lines 134.703 и 134.882 Å, which remained unresolved in the experiment with the LiF target because of the presence of neighbouring Li III lines. To estimate the resolving power in the vicinity of $\lambda = 135$ Å we recorded the spectrum of a teflon

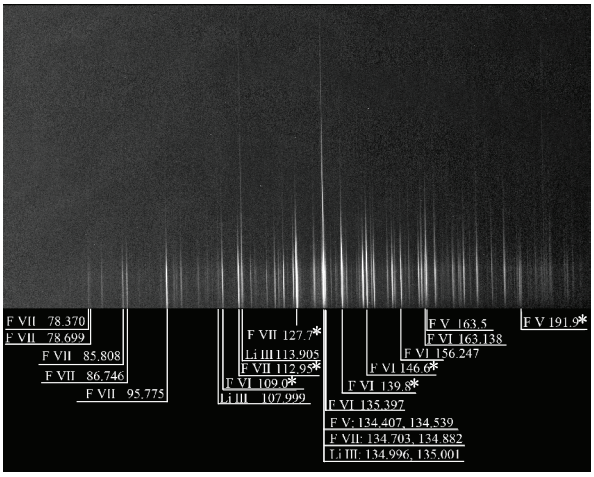

Figure 7. Spectrum of Li III and F V–F VII ions (target: LiF). The asterisk denotes unresolved line groups.

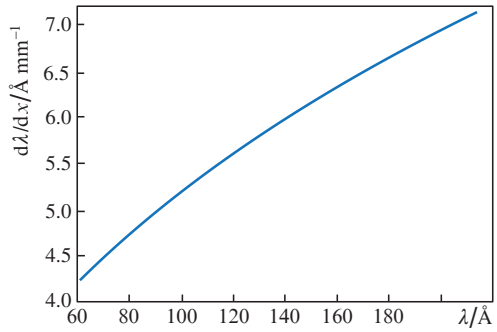

Figure 8. Plate scale of the VLS spectrograph.

$(-C_2F_4-)_n$ target, in which it was possible to resolve these lines. The resolving power of the instrument estimated from these lines was equal to ~750. Figure 9 displays the teflon spectrum digitised in the 133–136 Å interval by summing (binning) the counts of 10 detector pixels along the spectral lines.

Therefore, the implemented spectrograph possesses a resolving power of ~750 in the 135 Å region. Furthermore, resolved in the 166 Å region is a pair of F V ion lines, 165.983 Å and 166.177 Å, which corresponds to $\lambda/\delta\lambda \sim 860$. The design spectrometer characteristics agree nicely with the observed ones.

5. Conclusions

A compact (0.5-m long) flat-field VLS spectrograph for a range $\lambda \approx 50-275$ Å was implemented. The spectrograph was tested by recording the line spectra of multiply charged ions of lithium and fluorine excited in laser-produced plasma. The experimentally measured characteristics of the spectrograph are in perfect agreement with the design ones. Specifically, the spectral resolution corresponds to two detector pixels (26 μm). In particular, in the 135 Å wavelength region it is equal to 0.153 Å, which signifies a resolving power $\lambda/\delta\lambda \approx 880$.

In the selection of the method of spherical VLS-grating fabrication, we decided in favour of interference lithography. To this end, a lithographic configuration comprising an auxiliary aberrating mirror was calculated in the present work, i.e. the inverse problem of interference lithography was solved. The spatial frequency of interference fringes produced by the calculated

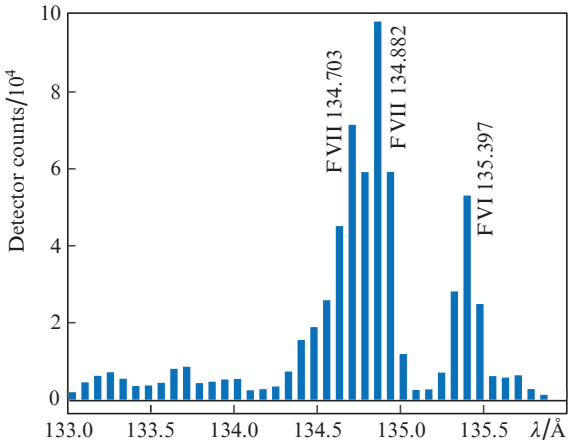

Figure 9. Histogram of the 133–136 Å portion of the teflon target spectrum. The F VII lines are safely resolved, which testifies to a resolving power of at least 750. The halwidth of the F VI ion line, which is equal to two detector pixels, corresponds to a resolving power of 880.

configuration faithfully approximated the polynomial (1) with parameters p_i from Table 1. The optical lithographic configuration was assembled in the State Institute of Applied Optics; the grating pattern was 'written' at a wavelength of 0.53 μm. The foundations were thereby laid for the domestic technology of SXR VLS-grating fabrication by interference lithography.

Acknowledgements. This work was supported by the Russian Science Foundation (Project No. 14-12-00506).

References

1. Kita T., Harada T., Nakano N., Kuroda H. *Appl. Opt.*, **22** (4), 512 (1983).
2. Nakano N., Kuroda H., Kita T., Harada T. *Appl. Opt.*, **23** (14), 2386 (1984).
3. Beiersdorfer P., Magee E.W., Träbert E., et al. *Rev. Sci. Instrum.*, **75** (10), 3723 (2004).
4. Dunn J., Magee E.W., Shepherd R., et al. *Rev. Sci. Instrum.,* **79**, 10E314 (2008).
5. Neely D., Chambers D., Danson C., et al. *AIP Conf. Proc.*, **426**, 479 (1998).
6. Koike M., Sano K., Gullikson E., Harada Y., Kumata H. *Rev. Sci. Instrum.*, **74** (2), 1156 (2003).
7. Imazono T., Koike M., Kawachi T., et al. *Appl. Opt.*, **51** (13), 2351 (2012).
8. Vishnyakov E.A., Kolesnikov A.O., Pirozhkov A.S., Ragozin E.N., Shatokhin A.N. *Quantum Electron.*, **48** (10), 916 (2018) [*Kvantovaya Elektron.*, **48** (10), 916 (2018)].
9. Imazono T., Ukita R., Nishihara H., Sasai H., Nagano T. *Appl. Opt.*, **57** (27), 7770 (2018).
10. Dvorak J., Jarrige I., Bisogni V., Coburn S., Leonhardt W. *Rev. Sci. Instrum.*, **87**, 115109-12 (2016).
11. Vishnyakov E.A., Shatokhin A.N., Ragozin E.N. *Quantum Electron.*, **45** (4), 371 (2015) [*Kvantovaya Elektron.*, **45** (4), 371 (2015)].
12. Vishnyakov E.A., Kolesnikov A.O., Kuzin A.A., Negrov D.V., Ragozin E.N., Sasorov P.V., Shatokhin A.N. *Quantum Electron.*, **47** (1), 54 (2017) [*Kvantovaya Elektron.*, **47** (1), 54 (2017)].
13. Shatokhin A.N., Kolesnikov A.O., Sasorov P.V., Vishnyakov E.A., Ragozin E.N. *Opt. Express*, **26** (15), 19009 (2018).
14. Vishnyakov E.A., Kolesnikov A.O., Ragozin E.N., et al. *Quantum Electron.*, **46** (10), 953 (2016) [*Kvantovaya Elektron.*, **46** (10), 953 (2016)].
15. Namioka T., Koike M. *Appl. Opt.*, **34** (13), 2180 (1995).
16. Vishnyakov E.A., Kirichenko A.S., Reva A.A., et al. *Proc. SPIE*, **9905**, 99053G (2016).
17. Vishnyakov E.A., Shcherbakov A.V., Pertsov A.A., et al. *Proc. SPIE*, **10235**, 102350W (2017).